

26. I. Provencio, H. M. Cooper, R. G. Foster, *J. Comp. Neurol.* **395**, 417 (1998).
27. J. Hannibal et al., *J. Neurosci.* **17**, 2637 (1997).
28. J. Hannibal, M. Moller, O. P. Ottersen, J. Fahrenkrug, *J. Comp. Neurol.* **418**, 147 (2000).
29. J. J. Gooley, J. Lu, T. C. Chou, T. E. Scammell, C. B. Saper, *Nature Neurosci.* **4**, 1165 (2001).
30. J. Hannibal, P. Hindersson, S. M. Knudsen, B. Georg, J. Fahrenkrug, *J. Neurosci.* **22**, 1 (RC191) (2002).
31. G. E. Pickard, *Neurosci. Lett.* **55**, 211 (1985).
32. M. E. Harrington, *Neurosci. Biobehav. Rev.* **21**, 705 (1997).
33. L. J. Trejo, C. M. Cicerone, *Brain Res.* **300**, 49 (1984).
34. R. J. Clarke, H. Ikeda, *Exp. Brain Res.* **57**, 224 (1985).
35. Single-letter abbreviations for the amino acid residues are as follows: A, Ala; C, Cys; D, Asp; E, Glu; F, Phe; G, Gly; H, His; I, Ile; K, Lys; L, Leu; M, Met; N, Asn; P, Pro; Q, Gln; R, Arg; S, Ser; T, Thr; V, Val; W, Trp; and Y, Tyr.
36. D. G. Green, N. V. Kapousta-Bruneau, *Vis. Neurosci.* **16**, 727 (1999).
37. F. A. Dunn, personal communication.
38. We thank R. R. Reed, and S. S. Wang and H. Zhao in his laboratory, for the tau-lacZ construct and invaluable advice. We also thank I. Provencio for providing the melanopsin BAC clone, J. Nathans and H. Sun for discussions, K. Takamiya, Y. Zhang, S. A. Ralls, M. Dehoff, B. E. Lonze, and especially M.

Cowan and the Johns Hopkins Transgenic Facility for technical help/advice in the generation of the tau-lacZ knock-in mice as well as providing the ES cells. We are grateful to R. Richardson and S. Carlson for technical assistance with the experiments on colocalization of melanopsin and intrinsic photic sensitivity. Finally, we thank R. Masland and members of the Yau laboratory, especially J. Bradley, W.-H. Xiong, and H. Zhong, for help/critique on the experiments. This work was supported by grants from the U.S. National Eye Institute to D.M.B. and K.-W.Y.

7 January 2002; accepted 11 January 2002

## Phototransduction by Retinal Ganglion Cells That Set the Circadian Clock

David M. Berson,\* Felice A. Dunn,† Motoharu Takao†

Light synchronizes mammalian circadian rhythms with environmental time by modulating retinal input to the circadian pacemaker—the suprachiasmatic nucleus (SCN) of the hypothalamus. Such photic entrainment requires neither rods nor cones, the only known retinal photoreceptors. Here, we show that retinal ganglion cells innervating the SCN are intrinsically photosensitive. Unlike other ganglion cells, they depolarized in response to light even when all synaptic input from rods and cones was blocked. The sensitivity, spectral tuning, and slow kinetics of this light response matched those of the photic entrainment mechanism, suggesting that these ganglion cells may be the primary photoreceptors for this system.

The SCN is the circadian pacemaker of the mammalian brain, driving daily cycles in activity, hormonal levels, and other physiological variables. Light can phase-shift the endogenous oscillator in the SCN, synchronizing it with the environmental day-night cycle. This process, the photic entrainment of circadian rhythms, originates in the eye and involves a direct axonal pathway from a small fraction of retinal ganglion cells to the SCN (1–3). A striking feature of this neural circuit is its apparent independence from conventional retinal phototransduction. In functionally blind transgenic mice lacking virtually all known photoreceptors (rods and cones), photic entrainment persists with undiminished sensitivity (4). Candidate photoreceptors for this system are nonrod, noncone retinal neurons, including some ganglion cells, that contain novel opsins or cryptochromes (5–8).

To determine whether retinal ganglion cells innervating the SCN are capable of phototransduction, we labeled them in the rat retina by retrograde transport of fluorescent microspheres injected into the hypothalamus

(9). In isolated retinas, whole-cell recordings were made of the responses of labeled ganglion cells to light (10) (Fig. 1, A to E). In most of these cells ( $n = 150$ ), light evoked large depolarizations with superimposed fast action potentials (Fig. 1, E to G) (11). The light response persisted during bath application of 2 mM cobalt chloride (Fig. 1F;  $n = 42$ ), which blocks calcium-mediated synaptic release from rods, cones, and other retinal neurons (12). In contrast, other ganglion cells prepared and recorded under identical conditions but not selectively labeled from the SCN (control cells) lacked detectable response to light even without synaptic blockade (47/50 cells; Fig. 1, I and J) (13). This is presumably because rod and cone photopigments were extensively bleached (10). A few control cells (3/50) exhibited weak, evanescent responses to light, but these were abolished by bath-applied cobalt ( $n = 2$ ).

To ensure blockade of conventional synaptic influences from rods and cones, we supplemented cobalt with a mixture of drugs that independently disrupted both the glutamatergic synapses crucial to vertical signal transfer through the retina and the ionotropic receptors responsible for most inhibitory influences on ganglion cells (14). Robust light responses persisted in SCN-projecting ganglion cells under these conditions (Fig. 1G;  $n = 7$ ). Furthermore, the somata of these

ganglion cells exhibited photosensitivity even when completely detached from the retina by microdissection (Fig. 1H;  $n = 3$ ). These light responses were not an artifact of photic excitation of either of the intracellular fluorophores we used, as the action spectrum of the light response (Fig. 2C) differed from the absorption spectra of both the retrograde tracer and Lucifer Yellow (LY) used for intracellular staining. Also, light-evoked increases in spike frequency were detectable in extracellular recordings, before patch rupture and LY dye filling ( $n = 5$ ). Whole-cell recordings revealed normal light responses when LY was omitted from the internal solution ( $n = 8$ ). In contrast, control cells lacked cobalt-resistant light responses even when labeled with both fluorescent beads and LY ( $n = 12$ ; Fig. 1I). These data indicate that retinal ganglion cells innervating the SCN are intrinsically photosensitive.

To determine if these cells could serve as the primary photoreceptors for circadian entrainment, we assessed congruence between their photic properties and those of the entrainment mechanism. The responses of a single cell to narrow-band stimuli of various intensities showed that at each wavelength, peak depolarization increased with stimulus energy (Fig. 2, A and B). Intensity-response curves exhibited a consistent slope when plotted in semilogarithmic coordinates (Fig. 2B), as expected for responses mediated by a single photopigment (principle of univariance). The horizontal displacements of the curves from one another reflect the spectral dependence of the pigment's quantum efficiency and yield the spectral sensitivity function shown in Fig. 2C (red curve). Other cells exhibited similar action spectra (Fig. 2C, green curve) (15). These action spectra closely matched that predicted for a retinal,  $\gamma$ -based pigment with peak sensitivity at 484 nm (Fig. 2C, black). They also resemble action spectra derived behaviorally for circadian entrainment in rodents (16, 17), as expected if these ganglion cells function as primary circadian photoreceptors (18). Judging from available spectral evidence, the photopigment in these ganglion cells is more likely to be a retinaldehyde-based opsin such as melanopsin (5, 19, 20) than a flavin-based cryptochrome (21).

Department of Neuroscience, Brown University, Providence, RI, 02912 USA.

\*To whom correspondence should be addressed. E-mail: David\_Berson@brown.edu

†These authors contributed equally to this work.

## REPORTS

The threshold and dynamic range of the light response in these ganglion cells were also similar to those of the entrainment mechanism. Threshold retinal irradiance for a full-field stimulus was about  $5 \times 10^{11}$  photons  $s^{-1} cm^{-2}$  at 500 nm ( $\sim \lambda_{max}$ ;  $n = 3$ ). This corresponds to an in vivo corneal irradiance of  $\sim 2 \times 10^{13}$  photons  $s^{-1} cm^{-2}$ , comparable to thresholds for circadian phase shifts in rodents ( $\sim 10^{10}$  to  $10^{13}$  photons  $s^{-1} cm^{-2}$  at 500 nm) (22–24) and to ocular illumination by the dawn sky. Response saturation in photosensitive ganglion cells occurred at irradi-

ances  $\sim 3$  logarithmic units above threshold (Figs. 2B and 3C), matching the dynamic range of entrainment behavior (16, 23, 24) and many SCN neurons [(25), but see (26)].

The circadian entrainment mechanism integrates light energy over very long time scales, exhibits little adaptation, and responds poorly to brief stimuli (24, 27). Similar features were evident in the behavior of photosensitive ganglion cells. Constant illumination depolarized cells tonically and elevated spike frequency, and the amount of depolarization was monotonically related to stimulus

energy (Fig. 3). Response kinetics were much slower than typical for ganglion cells. Latencies to response onset ( $V_m > 3$  standard deviations above baseline) were typically several seconds and ranged from several hundred milliseconds for saturating stimuli (Figs. 1F and 2A) to  $\sim 1$  min near threshold (Fig. 3B, bottom trace). Latencies from stimulus onset to peak depolarization were typically 10 to 20 s (range:  $\sim 2$  s to 2 min) and inversely

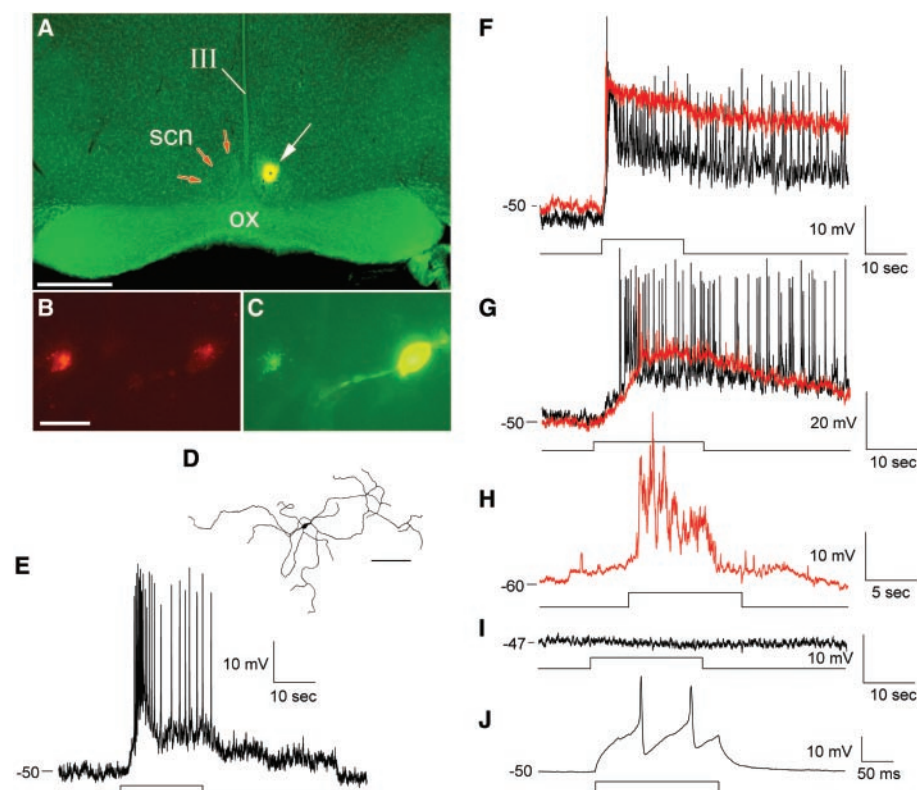


**Fig. 1.** Labeling and light responses of rat ganglion cells innervating the SCN. (A) Fluorescence photomicrograph showing deposit (white arrow) of mixed red and green fluorescent microspheres (appears as yellow) in the SCN. The red arrows mark boundaries of contralateral SCN. Acridine orange was used for green fluorescent Nissl counterstain. ox, optic chiasm; III, third ventricle. Scale bar, 500  $\mu m$ . (B) Two ganglion cells back-filled from the SCN, photographed in whole mount with rhodamine filter set to show retrograde labeling. The cell at right was patched and recorded. Scale bar, 20  $\mu m$ . (C) Same cells viewed under blue excitation, to show LY filling of the recorded cell. (D) Camera lucida drawing of cell filled in (C), as viewed in the whole mount after antibody to LY immunostaining (35). Scale bar, 100  $\mu m$ . (E) Strong depolarization and fast action potentials evoked in this cell (D) by a light pulse indicated by step in horizontal line below. (F to H) Evidence for the intrinsic photosensitivity of ganglion cells selectively retrolabeled from the SCN. (F and G) The light response apparent in control Ames solution (black traces) persisted during bath application of 2 mM  $CoCl_2$  (red traces) either alone (F) or in combination with a drug mixture blocking ionotropic and metabotropic glutamate receptors as well as ionotropic GABA and glycine receptors (G) (74). The absence of evoked spikes during drug application probably reflects depolarization block (tonic sodium channel inactivation) because weaker stimuli evoked spikes (40). (H) Light response recorded from the isolated soma of a ganglion cell retrolabeled from the SCN. The cell body was bathed in an enzyme solution (papain,  $\sim 20$  units/ml) with a puffer pipette and then mechanically removed from the retina with an empty patch pipette under visual control, amputating its dendrites and axon. (I and J) Control recordings from a conventional ganglion cell (Fig. 4C) labeled nonselectively by a deposit of rhodamine beads in the optic chiasm and filled with LY. Light evoked no detectable response (I), although synaptic transmission was not blocked and responses to current injection were normal (J) (+50 pA). Retinal irradiance of stimuli (in photons  $s^{-1} cm^{-2}$ ): (E)  $7 \times 10^{12}$ , (F)  $2.6 \times 10^{13}$ , (G)  $7.2 \times 10^{12}$ , (H)  $\sim 1 \times 10^{13}$ , and (I)  $\gg 9 \times 10^{13}$ . Stimuli in (E), (F), and (G) were 500 nm.

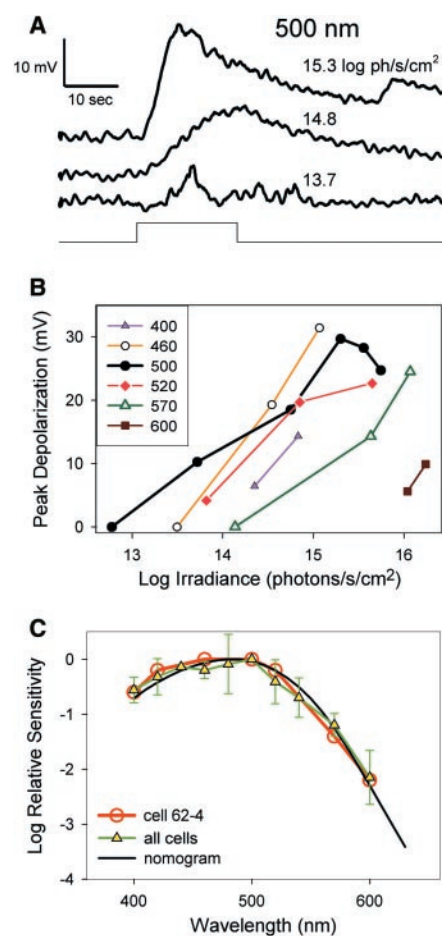


**Fig. 2.** Spectral tuning of light response in photosensitive ganglion cells. (A) Voltage responses of a single cell to a 500-nm narrow-band stimulus at indicated intensities (in  $\log_{10}$  photons  $s^{-1} cm^{-2}$ ). Baseline  $\sim -60$  mV for each trace. (B) Plots of peak depolarization as a function of log retinal irradiance for each of several narrow-band spectral lights (400- to 600-nm wavelength, as indicated; 10-nm width at half height); same cell as in (A). Peak was obtained from a 1-s boxcar average of raw voltages. (C) Spectral sensitivity functions derived for photosensitive ganglion cells from relative displacements of intensity-response functions along the abscissa in (B). Red curve: same cell as in (A) and (B). Green curve: group data for all cells ( $n = 34$ ; number of cells tested per wavelength as follows: 400 nm, 5; 420 nm, 3; 440 nm, 2; 460 nm, 4; 480 nm, 4; 500 nm, 34; 520 nm, 7; 540 nm, 5; 570 nm, 2; and 600 nm, 2). Black curve: nomogram for retinal, -based photopigment with  $\lambda_{max}$  of 484 nm (47), fit by least squares method to the group data.

REPORTS

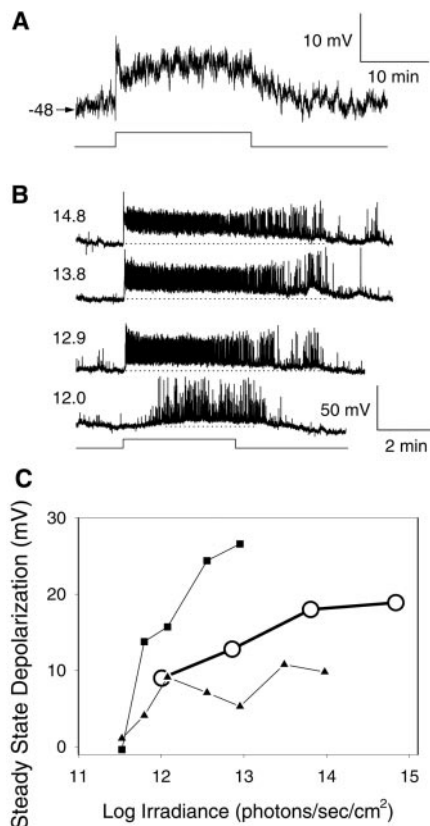
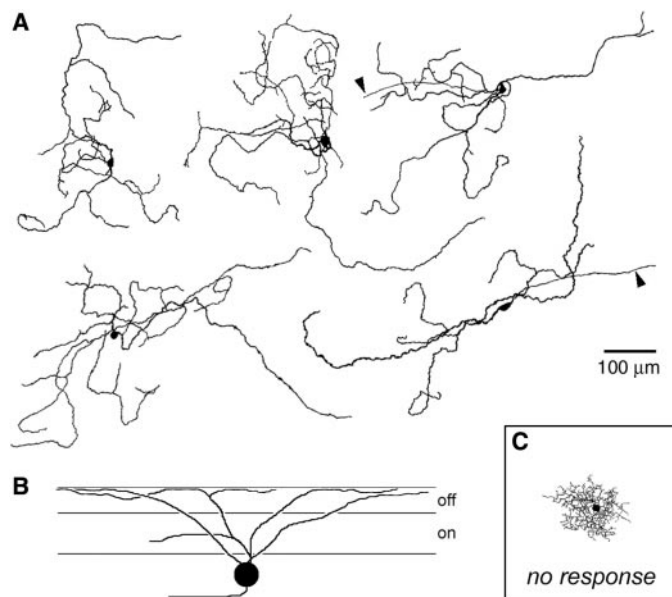


**Fig. 3.** Tonic encoding of light intensity by photosensitive ganglion cells. (A) Maintained depolarization evoked by 20 min of constant, diffuse illumination (retinal irradiance =  $3 \times 10^{13}$  photons  $s^{-1}$   $cm^{-2}$ ; 500 nm); spikes obscured by low sampling rate. (B) Voltage responses evoked in another cell by 4-min stimuli varying in intensity ( $\log_{10}$  irradiance in photons  $s^{-1}$   $cm^{-2}$  indicated at left; 500 nm). Note tonic depolarization, maintained spiking, and, for near-threshold stimulus (bottom trace), extremely long response latency. (C) Magnitude of maintained depolarization as a function of stimulus energy for the cell in (B) (open circles) and for two other cells. Bathing medium: Ames.

related to stimulus energy. Repolarization after intense stimuli required several minutes and was sometimes punctuated by spontaneous depolarizations and spike bursts lasting up to a minute each (Fig. 3B).

Photosensitive ganglion cells shared a common morphology (Fig. 4, A and B), as revealed by intracellular staining with LY (28). Somata were intermediate in diameter among neurons of the ganglion cell layer ( $14.7 \pm 1.2$   $\mu m$ , mean  $\pm$  SD;  $n = 18$ ). Many cells sent an axon into the optic fiber layer; those lacking one had presumably lost it during mechanical exposure of the soma before recording. The sparsely branching, tortuous dendrites of these cells arborized primarily in the outer part (OFF sublayer) of the inner plexiform layer (IPL; Fig. 4B). Although some dendrites coursed within the inner IPL (ON sublayer) for 100 to 200  $\mu m$ , nearly all terminated in the OFF sublayer. Such stratification is highly unusual for ganglion

**Fig. 4.** Morphology of photosensitive ganglion cells as revealed by intracellular staining. (A) Camera lucida drawings of cells stained with LY and viewed in retinal flat mounts. Arrowheads indicate axons. (B) Schematic summary of dendritic stratification of these cells, predominantly in the OFF sublayer of the inner plexiform layer. (C) Morphology of a control ganglion cell that lacked any light response under these conditions (Fig. 11). Scale bar applies to all panels.



cells depolarized by light [but see (29, 30)]. Dendritic fields were large (diameter  $497 \pm 115$   $\mu m$ ; mean  $\pm$  SD;  $n = 21$ ). Stimuli illuminating the dendrites but not the soma consistently evoked light responses (31). Control cells, which lacked cobalt-resistant light responses, had markedly different dendritic morphology (e.g., Fig. 4C).

These data identify a distinct ganglion cell type in the mammalian retina with characteristic dendritic profile and stratification pattern, extraordinarily sluggish and tonic light responses encoding ambient light level, and axonal projections to the SCN. The most striking feature of this cell type, however, is its apparent capacity for intrinsic phototransduction. The correspondences between the photic properties of these cells and those of the entrainment mechanism suggest that these unconventional ganglion cells may represent the primary photoreceptors for synchronizing the circadian clock to environmental time.

Melanopsin (5, 7) is probably the photopigment responsible for the intrinsic sensitivity of these cells to light, as it is selectively expressed in the small subset of ganglion cells that are intrinsically photosensitive and innervate the SCN (32, 33). In amphibians, certain nonretinal cells contain melanopsin, and these cells, too, are photosensitive, with action spectra resembling those of photosensitive rat ganglion cells (Fig. 2C) (5, 19, 20). Melanopsin exhibits marked sequence similarity to invertebrate opsins (5, 7), which, unlike vertebrate opsins, retain their photoisomerized retinaldehyde chromophore and typically trigger depolarizing light responses when activated. These properties may help to explain why photosensitive ganglion cells differ from conventional retinal photoreceptors in their response polarity and lack of dependence on the pigment epithelium. Cryptochromes, blue-light-absorbing, flavin-

based pigments, have been proposed as circadian photopigments (8), but spectral evidence (Fig. 2C) (21) weighs against their mediating the light response in intrinsically photosensitive ganglion cells.

*Note added in proof:* Further evidence for the presence of melanopsin in ganglion cells innervating the SCN has emerged (34).

References and Notes

1. R. Y. Moore, J. C. Spoh, J. P. Card, *J. Comp. Neurol.* **352**, 351 (1995).
2. T. Roenneberg, R. G. Foster, *Photochem. Photobiol.* **66**, 549 (1997).
3. M. von Schantz, I. Provencio, R. G. Foster, *Invest. Ophthalmol. Vis. Sci.* **41**, 1605 (2000).
4. M. S. Freedman et al., *Science* **284**, 502 (1999).
5. I. Provencio, G. Jiang, W. J. De Grip, W. P. Hayes, M. D. Rollag, *Proc. Natl. Acad. Sci. U.S.A.* **95**, 340 (1998).
6. D. Kojima, H. Mano, Y. Fukada, *J. Neurosci.* **20**, 2845 (2000).
7. I. Provencio et al., *J. Neurosci.* **20**, 600 (2000).
8. C. P. Selby, C. Thompson, T. M. Schmitz, R. N. Van Gelder, A. Sancar, *Proc. Natl. Acad. Sci. U.S.A.* **97**, 14697 (2000).
9. Methods conformed to NIH guidelines and were approved by Brown University's Institutional Animal Care and Use Committee. Rats (Sprague-Dawley, 56 to 70 days of age, 265 to 355 g;  $n = 256$ ) were anesthetized with ketamine [60 mg/kg intraperitoneal (ip)] and medetomidine (0.4 mg/kg ip). Fluorescent latex microspheres (rhodamine-labeled, alone or mixed with fluorescein-labeled microspheres; Lumafuor; 0.1 to 0.3  $\mu m$ ) were deposited unilaterally into the hypothalamus through glass pipettes tilted  $10^\circ$  from vertical. As expected (7), deposits involving the ventral hypothalamus but sparing the optic chiasm labeled from a few ganglion cells to as many as several hundred scattered over the retina. These cells are the focus of this report. Deposits spreading to the optic chiasm nonspecifically labeled thousands of ganglion cells, some of which were targeted for control recordings. Deposits involving overlying structures but sparing the SCN and chiasm labeled no ganglion cells.
10. Rats were anesthetized (Nembutal, 120 mg/kg ip) 2 to 28 days after tracer injection, and their eyes were removed and hemisected. Eyecups were rinsed in an enzyme solution [collagenase/dispase (2 mg/ml); DNAase (Sigma A1420; 0.1 mg/ml) in Ames medium, 1 min] to remove vitreous. Retinas were isolated, affixed to a cover slip with gelatin, vitreal surface up, and mounted in a chamber (Warner RC-26GLP). Retinas were maintained



at room temperature in bicarbonate-buffered Ames medium, and fluorescent-labeled cells were identified as described (35). Detachment from pigment epithelium and exposure to bright light during dissection ( $\sim 1 \times 10^{17}$  photons  $s^{-1} cm^{-2}$  measured at 500 nm) and epifluorescence examination ( $\sim 3 \times 10^{17}$  photons  $s^{-1} cm^{-2}$  at 560 nm) presumably strongly bleached rod and cone photopigments. Ganglion cell somata were exposed by microdissection. Whole-cell current clamp recordings were made with an intracellular amplifier (Cygnus Technologies DR-886, Delaware Water Gap, PA) and micropipettes (3 to 7 megaohms) containing 125 mM K-Gluconate, 5 mM NaCl, 4 mM KCl, 10 mM EGTA, 10 mM Hepes, 4 mM adenosine triphosphate—Mg, 7 mM phosphocreatine, 0.3 mM guanosine triphosphate—tris, LY (0.1% w/v), and biocytin (0.5% w/v). Resting potentials were not corrected for liquid junction potentials. Light stimuli were introduced from below with the microscope's 100-W tungsten-halogen lamp and transillumination optics. Neutral density and narrow-band interference filters (Oriol, Stratford, CT) controlled stimulus energy and wavelength. Energies were measured with a calibrated radiometer (UDT Instruments, Baltimore, MD). Except where noted, all stimuli were full-field and spectrally unfiltered.

11. The probability of obtaining such light responses was very high among back-filled cells in very sparsely labeled retinas but declined substantially when labeled ganglion cells totaled  $>100$ , presumably because involvement of the chiasm reduced labeling specificity. Peak depolarizations for saturating stimuli typically ranged from 15 to 30 mV.
12. Cobalt chloride was superfused at a concentration (2 mM in Ames) that blocks all light-evoked transmitter release from rods and cones in rat retina (36) and eliminates the otherwise robust light responses of ganglion cells in rat and cat eyecup preparations (37). Small chamber volume ( $<200 \mu l$ ) and inlet tubing dead space ( $<2 ml$ ) ensured complete exchange in minutes. Light responses also persisted when 2 mM  $[Co^{2+}]_o$  replaced 2 mM  $[Ca^{2+}]_o$  in a bath solution containing 126 mM NaCl, 3 mM KCl, 1.3 mM  $NaH_2PO_4$ , 2 mM  $MgSO_4$ , 26 mM  $NaHCO_3$ , and 10 mM dextrose ( $n = 2$ ).
13. In darkness, resting potentials of photosensitive ( $-46.7 \pm 14.8$  mV;  $n = 114$ ) and control ganglion cells ( $-48.5 \pm 11.0$  mV;  $n = 45$ ) were statistically indistinguishable ( $P > 0.2$ ;  $t$  test).
14. For most cells ( $n = 4$ ; including that shown in Fig. 1G), the drug solution consisted of 2 mM  $CoCl_2$ , 100  $\mu M$  L(+)-2-amino-4-phosphonobutyric acid to saturate and thus block signal transfer at Group III metabotropic glutamate receptors essential for photoreceptor-to-ON-bipolar cell transmission, 20  $\mu M$  6,7-dinitroquinoxaline-2,3-dione and 50  $\mu M$  DL-2-amino-5-phosphonovaleric acid to block ionotropic glutamate receptors [both *N*-methyl-D-aspartate (NMDA) and non-NMDA types] essential for communication between photoreceptors and OFF bipolar cells and between all bipolar cells and both amacrine and ganglion cells, and 50  $\mu M$  picrotoxin and 0.3  $\mu M$  strychnine to block ionotropic gamma-aminobutyric acid (GABA) and glycine receptors mediating most inhibition by amacrine cells. In two other cells, this cocktail was supplemented with 200  $\mu M$  hexamethonium bromide to block nicotinic acetylcholine receptors and either 500 or 2000  $\mu M$  1-octanol to block gap junctions; light-evoked depolarizations were not attenuated. Blockade typically enhanced depolarization (e.g., Fig. 1, F and G; mean depolarization = 18.5 mV in control medium and 26.7 mV during blockade;  $n = 7$ ). This may reflect increased membrane resistance due to loss of synaptic currents or of intrinsic calcium conductances. Resting potential was not significantly altered by synaptic blockade (means = 52.8 mV in Ames and 51.5 mV during blockade;  $n = 7$ ).
15. Sensitivity usually deteriorated noticeably within 30 to 120 min of break-in, probably because of cell dialysis ("run-down"). Group data in Fig. 2C (green curve) were therefore drawn only from responses obtained shortly after break-in, first at 500 nm and then at one other wavelength. Slow recovery kinetics necessitated long interstimulus intervals (3 min).

Thus, spectra for single cells were typically less complete than that shown for cell 62-4 (Fig. 2C, red curve). Nonetheless, the general form of the action spectrum was consistent. For example, among each of seven cells examined, the same rank order of sensitivity applied to the first three wavelengths tested: 500 nm  $>$  400 or 420 nm  $\gg$  570 or 600 nm.

16. J. S. Takahashi, P. J. DeCoursey, L. Bauman, M. Menaker, *Nature* **308**, 186 (1984).
17. I. Provencio, R. G. Foster, *Brain Res.* **694**, 183 (1995).
18. Differences between these physiological and behavioral curves may be attributable in part to spectral filtering by the lens, which presumably influenced the behavioral spectrum but not the data we obtained in isolated retina. Available spectral data do not exclude contributions of rods or green cones to the entrainment mechanism (17, 26).
19. L. Barr, M. Alpern, *J. Gen. Physiol.* **46**, 1249 (1963).
20. A. Daniolos, A. B. Lerner, M. R. Lerner, *Pigment Cell Res.* **3**, 38 (1990).
21. D. S. Hsu *et al.*, *Biochemistry* **35**, 13871 (1996).
22. Values are based on a 2-mm pupil and retinal area of 1.13  $cm^2$  (38). For comparison, absolute rod threshold in the rat is  $\sim 2 \times 10^{-4} cd/m^2$  [(39) as cited by (27)] or  $\sim 10^7$  photons  $cm^{-2} s^{-1}$  retinal irradiance.
23. O. Dkhissi-Benyahya, B. Sicard, H. M. Cooper, *J. Neurosci.* **20**, 7790 (2000).
24. D. E. Nelson, J. S. Takahashi, *Am. J. Physiol.* **277**, R1351 (1999).
25. J. H. Meijer, K. Watanabe, J. Schaap, H. Albus, L. Detari, *J. Neurosci.* **18**, 9078 (1998).
26. N. C. Aggelopoulos, H. Meissl, *J. Physiol.* **523** (part 1), 211 (2000).
27. D. E. Nelson, J. S. Takahashi, *J. Physiol.* **439**, 115 (1991).
28. Immunostaining for LY, avidin-biotin-peroxidase re-

action, and diaminobenzidine histochemistry were as described (35).

29. M. Pu, *J. Comp. Neurol.* **414**, 267 (1999).
30. ———, *J. Biol. Rhythms* **15**, 31 (2000).
31. Receptive fields were probed with spots or bars generated by placing an aperture in the microscope's spectrally unfiltered transilluminating tungsten beam and focusing it on the tissue with a  $\times 20$  objective lens. There was substantial spatial summation within the receptive field, but no surround antagonism, an otherwise ubiquitous feature of ganglion cell receptive fields.
32. S. Hattar, H.-W. Liao, M. Takao, D. M. Berson, K.-W. Yau, *Science* **295**, 1065 (2002).
33. J. J. Gooley, J. Lu, T. C. Chou, T. E. Scammell, C. B. Saper, *Nature Neurosci.* **4**, 1165 (2001).
34. J. Hannibal, P. Hindersson, S. M. Knudsen, B. Georg, J. Fahrénkrug, *J. Neurosci.* **22**, RC191 (2002).
35. M. Pu, D. M. Berson, *J. Neurosci. Methods* **41**, 45 (1992).
36. D. G. Green, N. V. Kapousta-Bruneau, *Vis. Neurosci.* **16**, 727 (1999).
37. F. A. Dunn, B. J. O'Brien, unpublished data.
38. A. Hughes, *Vision Res.* **19**, 569 (1979).
39. E. Dodt, K. Echte, *J. Neurophysiol.* **24**, 427 (1961).
40. D. M. Berson, F. A. Dunn, M. Takao, data not shown.
41. T. D. Lamb, *Vision Res.* **35**, 3083 (1995).
42. We thank B. Wooten for assistance with the spectral analysis; M. Seibert for help with the receptive field study; T. Nguyen for technical assistance; and H. Wässle, B. O'Brien, J. McIlwain, I. Provencio, M. Slaughter, and L. Peichl for their valuable comments on the manuscript. Supported by NIH grant EY12793 to D.M.B.

18 October 2001; accepted 7 January 2002

## Metabolic Enzymes of Mycobacteria Linked to Antioxidant Defense by a Thioredoxin-Like Protein

R. Bryk,<sup>1,4\*</sup> C. D. Lima,<sup>2,5\*</sup> H. Erdjument-Bromage,<sup>3</sup> P. Tempst,<sup>3,5,6</sup> C. Nathan<sup>1,4,6†</sup>

*Mycobacterium tuberculosis* (Mtb) mounts a stubborn defense against oxidative and nitrosative components of the immune response. Dihydrolipoamide dehydrogenase (Lpd) and dihydrolipoamide succinyltransferase (SucB) are components of  $\alpha$ -ketoacid dehydrogenase complexes that are central to intermediary metabolism. We find that Lpd and SucB support Mtb's antioxidant defense. The peroxiredoxin alkyl hydroperoxide reductase (AhpC) is linked to Lpd and SucB by an adaptor protein, AhpD. The 2.0 angstrom AhpD crystal structure reveals a thioredoxin-like active site that is responsive to lipoamide. We propose that Lpd, SucB (the only lipoyl protein detected in Mtb), AhpD, and AhpC together constitute a nicotinamide adenine dinucleotide (reduced)-dependent peroxidase and peroxynitrite reductase. AhpD thus represents a class of thioredoxin-like molecules that enables an antioxidant defense.

Mtb, the leading cause of death from a single bacterial species, is restrained from proliferation in most infected individuals by oxidative and nitrosative stress imposed in part by inducible nitric oxide synthase (1, 2). Yet despite the immune response, viable mycobacteria persist. Bacterial persistence has directed our attention to Mtb's defenses against oxidative and nitrosative stress.

Mtb peroxiredoxin alkyl hydroperoxide reductase (AhpC), a member of the peroxiredoxin family of nonheme peroxidases, protects heterologous bacterial and human cells against oxidative and nitrosative injury (3, 4). The redundancy of peroxiredoxins in Mtb complicates interpretation of the phenotype of an *ahpC*-deficient mutant (5). AhpC metabolizes peroxides (6) and peroxynitrite (7) via a conserved